

**Hydrodynamics of chiral squirmers**P. S. Burada<sup>1,\*</sup>, R. Maity,<sup>1</sup> and F. Jülicher<sup>2</sup><sup>1</sup>*Department of Physics, Indian Institute of Technology Kharagpur, Kharagpur 721302, India*<sup>2</sup>*Max Planck Institute for the Physics of Complex Systems, Nöthnitzer Str. 38, 01187 Dresden, Germany* (Received 20 May 2021; revised 15 November 2021; accepted 1 February 2022; published 14 February 2022)

Many microorganisms take a chiral path while swimming in an ambient fluid. In this paper we study the combined behavior of two chiral swimmers using the well-known squirmer model taking into account chiral asymmetries. In contrast to the simple squirmer model, which has an axisymmetric distribution of slip velocity, the chiral squirmer has additional asymmetries in the surface slip, which contribute to both translations and rotations of the motion. As a result, swimming trajectories can become helical and chiral asymmetries arise in the flow patterns. We study the swimming trajectories of a pair of chiral squirmers that interact hydrodynamically. This interaction can lead to attraction and repulsion, and in some cases even to bounded states where the swimmers continue to periodically orbit around a common average trajectory. Such bound states are a signature of the chiral nature of the swimmers. Our study could be relevant to the collective movements of ciliated microorganisms.

DOI: [10.1103/PhysRevE.105.024603](https://doi.org/10.1103/PhysRevE.105.024603)**I. INTRODUCTION**

Understanding the locomotion and the swimming behavior of biological microswimmers has drawn substantial attention from scientists [1–7]. There exists a rich literature exploring the novel phenomena emerging from cellular motility at the submillimeter scale [8–10]; nutrient transport [11,12], stochastic dancing of *Volvox* algae [13–15], formation of biofilm [16–19], stochastic swimming [20–22], swimming of sperm cells [5,23,24] are a few examples. These studies have inspired the design of artificial microswimmers for microsurgery and targeted drug delivery [25]. Different microswimmers employ different motility mechanisms to swim in a fluid. We are motivated by motion based on ciliary propulsion of many microorganisms.

Many ciliated microorganisms can actively swim due to the periodic motion of hair-like appendages such as motile cilia attached on their surface [26]. Swimming corresponds to a net motion, relative to the background fluid, resulting from nonreciprocal shape changes of the swimmer [27–29]. The beating of cilia on the surface of organisms such as *Paramecium* or *Opalina* generates intricate wave patterns, called metachronal waves, which enable the body to swim in a fluid [30]. In addition to biological swimmers, artificial microswimmers have recently attracted much interest. Several artificial microswimmers use different self-propulsion mechanisms that involve the generation of surface flows [21,31–38].

The hydrodynamics of the resulting propulsion was studied with a simple model called squirmer, introduced by Lighthill [1] and further developed by Blake and others [2,39]. A squirmer is a spherical object moving in a fluid, driven by a

pattern of slip velocity on its surface. Such a squirmer is force free, but is associated with a force dipole. As a result, the squirmer can swim in the fluid and generate a characteristic hydrodynamic flow pattern. Though the squirmer was first developed as a model to understand ciliary propulsion, it is now widely used to study other types of microswimmers broadly classified as pullers and pushers [6,40]. While pullers have an extensile force dipole, resulting, e.g., from the front part of the body, pushers have a contractile force dipole stemming, e.g., from the rear part of the body [7].

In simple versions of the squirmer model, the surface slip of the squirmer is axisymmetric [1,2] which leads to swimming in a direction along the axis of symmetry. Many microswimmers, for example, marine zooplankton, propel along a chirally asymmetric path and generate flow field nonaxisymmetric in nature. Such chiral swimmers exhibit rotational motion and often move along helical paths [23,24,41–44]. A recent experimental study shows that artificially designed swimmers which are generating chiral flow, propel along a helical path in a surfactant solution [45]. Understanding the role of chirality in the motility of microswimmers has therefore drawn significant attention [46–52]. Many biological phenomena, e.g., plankton bloom in ocean [53], nutrient uptake by swimming organisms, bioconvection [54,55], transient clustering [56], cancer and tissue development [57], amoebae aggregation due to starvation [58] result from the collective motion of microorganisms and motile cells. For example, hydrodynamic bound states have been discussed when a pair of bottom-heavy *Volvox* swimming near a substrate [13–15]. Therefore, it is important to understand the results of interactions between swimmers for example via the generalized flows.

In this paper, we briefly discuss the general chiral squirmer model and derive the solution of the hydrodynamic flow field around the body. We then study the motion of a pair of chiral

\*Corresponding author: [psburada@phy.iitkgp.ac.in](mailto:psburada@phy.iitkgp.ac.in)

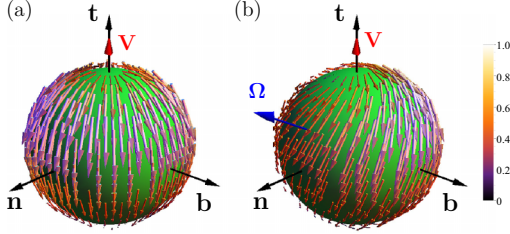


FIG. 1. Examples of surface slip velocity patterns of a simple squirmer (a) and a chiral squirmer (b) in the body-fixed reference frame  $\mathbf{n}$ ,  $\mathbf{b}$ , and  $\mathbf{t}$ . Parameter values are  $\mathbf{V} = v(0, 0, 1)$ ,  $\mathbf{\Omega} = v(1/\sqrt{2}, 0, 1/\sqrt{2})/a$ , and  $\beta_{20}^r = v/3$ . For the simple squirmer (axisymmetric),  $\gamma_{20}^r = 0$  and for the chiral squirmer  $\gamma_{20}^r = v/3$ . All other coefficients are set to zero.

squirmers that exhibit complex swimming trajectories as they interact via the hydrodynamic flow field. The rest of this article is organized as follows. In Sec. II we introduce the chiral squirmer model and the governing equations. Hydrodynamics of a single chiral squirmer is discussed in Sec. III. The combined behavior of two chiral squirmers is presented in Sec. IV. The main conclusions are provided in Sec. VI.

## II. HYDRODYNAMIC FLOW OF A SQUIRMER

To discuss the swimming of microorganisms in the low Reynolds number regime, inertial forces can be neglected. In an incompressible, Newtonian fluid, the hydrodynamic flow field obeys the Stokes equation [59],

$$\eta \nabla^2 \mathbf{u} = \nabla p, \quad (1)$$

where  $\eta$  is the viscosity,  $\mathbf{u}$  is the velocity field, and  $p$  is the pressure field which plays the role of a Lagrange multiplier to impose the incompressibility constraint  $\nabla \cdot \mathbf{u} = 0$ .

A squirmer is a rigid spherical body of radius  $a$ . On its surface, we prescribe a surface slip velocity  $\mathbf{S}(\theta, \phi)$  which is tangential to the surface and parameterized by the polar and azimuthal angle  $\theta$  and  $\phi$ , respectively, in a body-fixed frame. The latter is defined by three orthogonal unit vectors attached to the sphere center  $\mathbf{n}$ ,  $\mathbf{b}$ , and  $\mathbf{t}$ ; see Fig. 1. It is convenient to express this surface slip pattern using gradients of spherical harmonics that form a basis for tangential vectors on the surface [59]. The slip velocity can then be expressed in the form

$$\begin{aligned} \mathbf{S}(\theta, \phi) = & \sum_{l=1}^{\infty} \sum_{m=-l}^l \left\{ -\beta_{lm} \nabla_s [P_l^m(\cos \theta) e^{im\phi}] \right. \\ & \left. + \gamma_{lm} \hat{\mathbf{t}} \times \nabla_s (P_l^m(\cos \theta) e^{im\phi}) \right\}, \end{aligned} \quad (2)$$

where  $\nabla_s$  is the gradient operator on the surface of the sphere defined as  $\nabla_s = \mathbf{e}_\theta \partial/\partial\theta + (1/\sin\theta) \mathbf{e}_\phi \partial/\partial\phi$ ,  $\hat{\mathbf{t}}$  is the unit vector in the radial direction,  $P_l^m(\cos\theta) e^{im\phi}$  are non-normalized spherical harmonics, where  $P_l^m(\cos\theta)$  denotes Legendre polynomials. The complex coefficients  $\beta_{lm}$  and  $\gamma_{lm}$  are the mode amplitudes of the prescribed surface slip velocity. We introduce the real and imaginary parts of these amplitudes as  $\beta_{lm} = \beta_{lm}^r + im\beta_{lm}^i$  and  $\gamma_{lm} = \gamma_{lm}^r + im\gamma_{lm}^i$  with complex conjugates  $\beta_{lm}^* = (-1)^m \beta_{l,-m}$  and  $\gamma_{lm}^* = (-1)^m \gamma_{l,-m}$ , respectively.

The velocity and rotation rate can be calculated directly from the surface slip profile Eq. (2) [60]. They can be expressed in the body fixed reference frame as  $\mathbf{V} = 2(\beta_{11}^r, \beta_{11}^i, \beta_{10}^r)/3$  and  $\mathbf{\Omega} = (\gamma_{11}^r, \gamma_{11}^i, \gamma_{10}^r)/a$ , respectively. Without loss of generality, we can choose the body-fixed reference frame  $(\mathbf{n}, \mathbf{b}, \mathbf{t})$  such that  $\mathbf{t}$  points in the direction of motion. With this choice, we have  $\beta_{11}^r = \beta_{11}^i = 0$  and we write  $\beta_{10}^r = 3v/2$  such that  $v = |\mathbf{V}|$  is the speed of the swimmer. The translation velocity, the rotation rate, and the rate of energy dissipation  $Q$  in the flow field can then be expressed as [60],

$$\mathbf{V} = v \mathbf{t}, \quad (3)$$

$$\mathbf{\Omega} = \frac{\gamma_{11}^r}{a} \mathbf{n} + \frac{\gamma_{11}^i}{a} \mathbf{b} + \frac{\gamma_{10}^r}{a} \mathbf{t}, \quad (4)$$

$$Q = 12\pi a \eta \left( v^2 + \frac{4a^2}{9} |\mathbf{\Omega}|^2 \right). \quad (5)$$

Equation (5) reveals that a chiral squirmer dissipates more energy than a nonchiral one due to additional flows associated with rotations.

In Eq. (2) the modes of surface slip described by  $\gamma_{lm}$  (for  $m \neq 0$ ) break the axial symmetry of the flow profile. For the case  $\gamma_{lm} = 0$ , the swimmer is nonchiral because modes corresponding to the coefficients  $\beta_{lm}$  do not generate an azimuthal part of the flow field. Considering only the modes  $\beta_{10}$  in Eq. (2), setting all other modes to zero, one recovers the axisymmetric squirmer model which generates translational motion only [1,2]. Figure 1(a) shows an example of such an axisymmetric surface slip pattern. The former pattern is axisymmetric concerning the  $\mathbf{t}$  axis. An example of the asymmetric surface slip of a chiral squirmer is shown in Fig. 1(b).

## III. HYDRODYNAMICS OF A SINGLE CHIRAL SQUIRMER

### A. Hydrodynamic flow field

For the prescribed surface slip of the chiral squirmer, we can calculate the corresponding flow field. Using a laboratory reference frame (lf) which is at rest with respect to the fluid away from the swimmer, the flow field, the pressure field, and the vorticity are obtained as

$$\begin{aligned} \mathbf{u}_{\text{lf}}(\mathbf{r}) = & \frac{3v}{2} \frac{a^3}{r^3} \left[ P_1(\mathbf{t} \cdot \hat{\mathbf{r}}) \hat{\mathbf{r}} - \frac{\mathbf{t}}{3} \right] + 3\beta_{20}^r \left( \frac{a^4}{r^4} - \frac{a^2}{r^2} \right) P_2(\mathbf{t} \cdot \hat{\mathbf{r}}) \hat{\mathbf{r}} \\ & + \beta_{20}^r \frac{a^4}{r^4} P_2'(\mathbf{t} \cdot \hat{\mathbf{r}}) [(\mathbf{t} \cdot \hat{\mathbf{r}}) \hat{\mathbf{r}} - \mathbf{t}] - \gamma_{20}^r \frac{a^3}{r^3} P_2'(\mathbf{t} \cdot \hat{\mathbf{r}}) \mathbf{t} \times \hat{\mathbf{r}}, \end{aligned} \quad (6)$$

$$p_{\text{lf}}(\mathbf{r}) = -2\eta \beta_{20}^r \frac{a^2}{r^3} P_2(\mathbf{t} \cdot \hat{\mathbf{r}}), \quad (7)$$

$$\boldsymbol{\omega}_{\text{lf}}(\mathbf{r}) = \frac{\nabla \times \mathbf{u}_{\text{lf}}(\mathbf{r})}{2}, \quad (8)$$

where  $\mathbf{t}$  is the swimming direction,  $r$  is the distance from the center of the swimmer where the flow field is determined,  $\hat{\mathbf{r}} = \mathbf{r}/r$  is the radial vector,  $P_2(x)$  denotes a second-order Legendre polynomial, and  $P_2' = dP_2/dx$  with  $x = \mathbf{t} \cdot \hat{\mathbf{r}} = \cos\theta$ . Note that in Eq. (6) we have written terms only up to  $l = 2$  and do not consider higher order contributions, since they

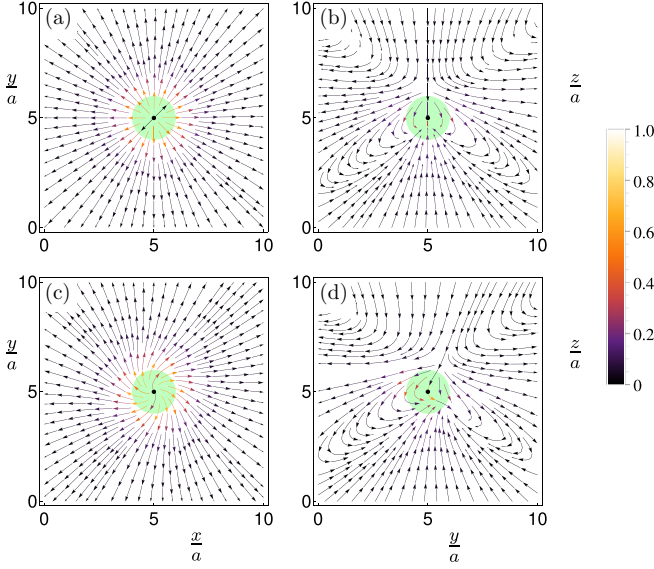


FIG. 2. Velocity flow fields are generated in the laboratory frame by a squirmer [top panels, (a) and (b)] and a chiral squirmer [bottom panels, (c) and (d)]. The velocity profiles are projected on  $xy$  plane for  $z = a$  (left panels), and on  $yz$  plane for  $x = a$  (right panels). The planes are shown to touch the squirmer (indicated in green) at the black dot. Parameter values are  $\mathbf{V} = v(0, 0, 1)$ ,  $\mathbf{\Omega} = v(1/\sqrt{2}, 0, 1/\sqrt{2})/a$ , and  $\beta_{20}^r = v$ . For the simple squirmer (axisymmetric),  $\gamma_{20}^r = 0$  and for the chiral squirmer  $\gamma_{20}^r = v$ . All other parameters are set to zero. The color code provides the magnitude of the flow field.

decay more rapidly with  $r$ . Additionally, to have a minimal model, we have ignored  $l = 2$  modes with  $m \neq 0$ . However, it is straightforward to include the additional terms in the analysis. Note that in Eq. (6), the terms  $o(1/r^4)$  decay faster than lower order terms, and hence their contribution is negligible to the flow field at a large distance. The flow field in the body frame (bf) can be obtained from that in the laboratory frame (lf) as  $\mathbf{u}_{bf}(\mathbf{r}) = \mathbf{u}_{lf}(\mathbf{r}) - \mathbf{V} - \mathbf{\Omega} \times \mathbf{r}$ .

Figure 2 depicts examples of the laboratory frame flow field generated by a simple squirmer [top panels, Figs. 2(a) and 2(b)] and by a chiral squirmer [bottom panels, Figs. 2(c) and 2(d)]. The flows shown are projected on planes that touch the squirmer at one point (black dots). The flow field of a simple squirmer is axially symmetric concerning the  $z$  axis, i.e., the direction of propulsion [Fig. 2(a)]. The flow pattern in the  $yz$  plane is mirror symmetric to the  $x$  and  $y$  axes [Figs. 2(a) and 2(b)]. In contrast, the chiral squirmer produces a rotational flow around the  $z$  axis with clockwise sense of rotation when viewed from the top for  $z > 0$  [Fig. 2(c)] and counterclockwise for  $z < 0$  (not shown). Note that for  $z = 0$ , no chiral component exists in the flow. In the  $yz$  plane, there is no mirror symmetry as a result of chirality [Fig. 2(d)]. Also note that the  $l = 1$  modes do not generate chiral flow patterns. However, they generate a body rotation  $\mathbf{\Omega}$  of the chiral squirmer. Chiral contributions to the flow stem from terms with  $l \geq 2$  such as the contribution with the term  $\sim \gamma_{20}^r/r^3$  in Eq. (6). The dominant term in the far field is proportional to  $\sim \beta_{20}^r/r^2$ , which corresponds to a Stokes doublet and implies the action of a force dipole on the fluid [2]. Thus, for  $\beta_{20}^r/\beta_{10}^r > 0$  the

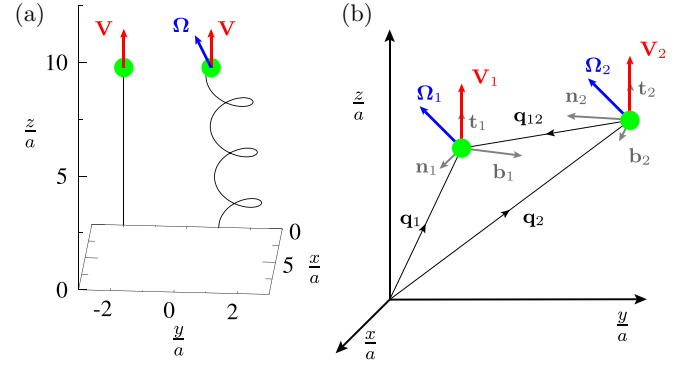


FIG. 3. (a) Swimming path of a squirmer (straight line) and a chiral squirmer (helix) for the same parameter values as in Fig. 1. The swimming velocity and the rotation rate are indicated. (b) Schematic representation of two chiral squirmers in the laboratory frame of reference.

chiral squirmer is a puller and for  $\beta_{20}^r/\beta_{10}^r < 0$ , it is a pusher. For an illustration, see the 3D flow field of a puller and pusher in Figs. 4(a) and 4(b).

### B. Path of a chiral squirmer

The equations of motion of the chiral squirmer determining the swimming path  $\mathbf{q}(t)$  and its instantaneous orientation  $(\mathbf{n}, \mathbf{b}, \mathbf{t})$  read in the laboratory frame,

$$\dot{\mathbf{q}} = \mathbf{V}, \quad \begin{bmatrix} \dot{\mathbf{n}} \\ \dot{\mathbf{b}} \\ \dot{\mathbf{t}} \end{bmatrix} = \mathbf{\Omega} \times \begin{bmatrix} \mathbf{n} \\ \mathbf{b} \\ \mathbf{t} \end{bmatrix}, \quad (9)$$

where the dots denote time derivatives. For time-independent coefficients  $\beta_{lm}$  and  $\gamma_{lm}$ ,  $\mathbf{V}$  and  $\mathbf{\Omega}$  are constant when described in the body frame. The angle  $\chi$  between  $\mathbf{V}$  and  $\mathbf{\Omega}$  obeys  $\chi = \cos^{-1}(\frac{\mathbf{V} \cdot \mathbf{\Omega}}{|\mathbf{V}||\mathbf{\Omega}|})$ . For  $\mathbf{V} \parallel \mathbf{\Omega}$ , we get  $\chi = 0$ , and the resulting swimming path is a straight line; see Fig 3(a). In this case, the swimmer rotates around the axis of motion. For  $\chi = \pi/2$ , the chiral squirmer moves in a circular path in a plane (not shown). For other values of  $\chi$ , the path of a chiral squirmer is a helix; see Fig 3(a). Using the velocity and rotation rate of the swimmer, one can calculate the curvature  $\kappa_0 = |\mathbf{\Omega} \times \mathbf{V}|/|\mathbf{V}|^2$  and the torsion  $\tau_0 = |\mathbf{\Omega} \cdot \mathbf{V}|/|\mathbf{V}|^2$  or alternatively the radius  $r_0 = \kappa_0/(\kappa_0^2 + \tau_0^2)$  and the pitch  $p_0 = \tau_0/(\kappa_0^2 + \tau_0^2)$  of the helical swimming path. Without loss of generality, we assume that the squirmer rotates in the  $\mathbf{n}$ - $\mathbf{t}$  plane, i.e., we set  $\gamma_{11}^i = 0$  in Eq. (4), with the magnitude  $|\mathbf{\Omega}| = v/a$ . With this choice, we can write its components as  $\gamma_{11}^r/a = (v/a) \sin \chi$ ,  $\gamma_{11}^i/a = 0$ , and  $\gamma_{10}^r/a = (v/a) \cos \chi$ .

## IV. HYDRODYNAMIC INTERACTION OF TWO CHIRAL SQUIRMERS

Having discussed the flow field and motion of a chiral squirmer in the laboratory frame, we can now focus on the motion of a pair of hydrodynamically interacting chiral squirmers. We consider the situation where the swimmers are far apart than their diameter; subsequently, the superposition of the flow fields can provide an excellent approximation to

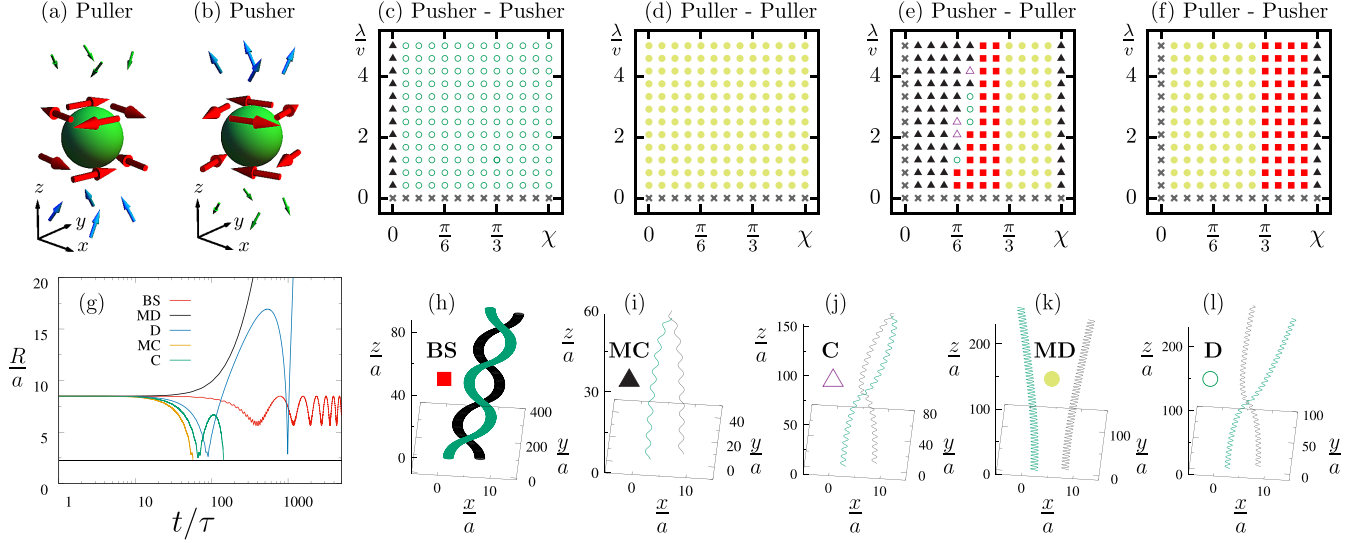


FIG. 4. [(a), (b)] Flow around a puller and a pusher. [(c)–(f)] Represent the numerically obtained swimming behaviors (states) of a pair of hydrodynamically interacting chiral squirmers. Different symbols represent different states. Square symbol = bounded state (BS), closed circles = monotonic divergence state (MD), open circles = divergence state (D), closed triangles = monotonic convergence state (MC), open triangles = convergence state (C), and cross symbols represent the situation where swimmers move parallel to each other. The initial positions for the swimmers are set to  $\mathbf{q}_1 = (9, 9, 0)a$  and  $\mathbf{q}_2 = (3, 3, 0)a$ . Swimmers have the same initial velocity  $\mathbf{V}_1 = \mathbf{V}_2 = v(0, 0, 1)$  and rotation rate  $\mathbf{\Omega}_1 = \mathbf{\Omega}_2 = v(\cos \chi, 0, \sin \chi)/a$ , which depends on the angle  $\chi$ . [(h)–(l)] The corresponding trajectories of the states, for the values  $\chi = \pi/3$  and  $(\lambda_1, \lambda_2) = v(1, -1)$  for BS,  $\chi = 5\pi/12$  and  $(\lambda_1, \lambda_2) = v(-2, 2)$  for MC,  $\chi = \pi/6$  and  $(\lambda_1, \lambda_2) = v(-2, 2)$  for C,  $\chi = \pi/3$  and  $(\lambda_1, \lambda_2) = v(-1, 1)$  for MD, and  $\chi = 5\pi/12$  and  $(\lambda_1, \lambda_2) = v(-1, -1)$  for D. (g) The corresponding distance  $R$ , scaled by the radius of the swimmer  $a$ , between the swimmers is plotted as a function of time  $t$ , scaled by  $\tau = v/a$ .

the combined flow and permits to study hydrodynamic interactions [39]. As a result, a given chiral swimmer obtains an additional contribution to its velocity and rotation rate due to the flow field induced by the other swimmer. Thus, the equations of motion for swimmer 1 in the presence of swimmer 2 read

$$\begin{aligned} \dot{\mathbf{q}}_1 &= \mathbf{V}_1 + \mathbf{u}_2(\mathbf{q}_{12}, \mathbf{n}_2, \mathbf{b}_2, \mathbf{t}_2), \\ \begin{bmatrix} \dot{\mathbf{n}}_1 \\ \dot{\mathbf{b}}_1 \\ \dot{\mathbf{t}}_1 \end{bmatrix} &= [\mathbf{\Omega}_1 + \mathbf{\omega}_2(\mathbf{q}_{12}, \mathbf{n}_2, \mathbf{b}_2, \mathbf{t}_2)] \times \begin{bmatrix} \mathbf{n}_1 \\ \mathbf{b}_1 \\ \mathbf{t}_1 \end{bmatrix}, \end{aligned} \quad (10)$$

where  $\mathbf{u}_2(\mathbf{q}_{12}, \mathbf{n}_2, \mathbf{b}_2, \mathbf{t}_2)$  and  $\mathbf{\omega}_2(\mathbf{q}_{12}, \mathbf{n}_2, \mathbf{b}_2, \mathbf{t}_2)$  are the velocity field and vorticity created by swimmer 2 at the position of swimmer 1, as in Eqs. (6) and (8). The time-dependent distance between the swimmers is given by  $R = |\mathbf{q}_{12}| = |\mathbf{q}_1 - \mathbf{q}_2|$ ; see Fig. 3(b). A corresponding equation holds for swimmer 2. Therefore, we see that the unperturbed velocity and rotation rate of a swimmer gets modified due to the velocity field and vorticity, respectively, of the other swimmer.

Using Eq. (10), we numerically calculate the trajectories of a pair of chiral swimmers and investigate their combined behavior; see Fig. 4. We consider chiral swimmers having translational velocities of equal magnitudes, i.e.,  $|\mathbf{V}_1| = |\mathbf{V}_2| = v$ . The rotation rates of the swimmers are in general different and read  $\mathbf{\Omega}_1 = v(\sin \chi_1, 0, \cos \chi_1)/a$  for swimmer 1 and  $\mathbf{\Omega}_2 = v(\sin \chi_2, 0, \cos \chi_2)/a$  for swimmer 2. Modification in  $\chi_1$  and  $\chi_2$  changes the corresponding torsion and curvature of the swimmers' helical trajectories. Additionally, the flow field of one swimmer influences the motion of the

other swimmer. As mentioned earlier,  $l > 1$  modes in the velocity field, Eq. (6), play a vital role in the hydrodynamic interaction between the swimmers. Thus, we choose the  $l = 2$  modes corresponding to swimmer 2 as  $3\beta_{20}^r = 3\gamma_{20}^r = \lambda_1$  and similarly for swimmer 2 as  $3\beta_{20}^r = 3\gamma_{20}^r = \lambda_2$ . Note that for  $\lambda_1 \neq \lambda_2$ , the swimmers differ in their chiral flows that they generate. Thus, variation in  $\chi_i$  and  $\pm\lambda_i$  ( $i = 1, 2$ ) determine the nature of the interaction between the chiral squirmers and gives rise to several interesting swimming characteristics. We have considered various possible initial configurations for the swimmers. Here we present only the planar configuration, where both the swimmers start initially on the  $xy$  plane, separated by a distance  $d$ , moving in the positive  $z$  direction. This particular choice of the configuration recovers the known behaviors exhibited by two simple squirmers (without chirality) and some additional exciting behaviors discussed below. Note that swimmers get enough time to interact in this configuration, whereas it may not be the case in other configurations.

#### A. State diagram in the $\chi$ - $\lambda$ plane

We start from initial positions  $\mathbf{q}_1 = (9, 9, 0)a$  and  $\mathbf{q}_2 = (3, 3, 0)a$  of the squirmers with  $\mathbf{t}_1$  and  $\mathbf{t}_2$  in the  $z$  direction, and  $\mathbf{n}_1$  and  $\mathbf{n}_2$  in the  $x$  direction. Note that the distance between the swimmers is larger than the radius  $a$  of the swimmers. We choose  $\chi = \chi_1 = \chi_2$ , i.e., the relative orientations of the swimmers with respect to their motion are the same, and  $\lambda = |\lambda_1| = |\lambda_2|$ , i.e., the strength of the hydrodynamic flow fields of both the swimmers are identical. Consider the subcases, i.e., pusher-pusher:  $(-\lambda_1, -\lambda_2)$ , puller-puller:  $(\lambda_1, \lambda_2)$ ,

pusher-puller:  $(-\lambda_1, \lambda_2)$ , and puller-pusher:  $(\lambda_1, -\lambda_2)$ . Thus, by varying the strengths of  $\chi$  and  $\lambda$ , we have observed different behaviors of two hydrodynamically interacting swimmers; see Fig. 4. For example, (1) bounded state (BS), where the swimmers spiral around each other and move synchronously with a distance that changes periodically, (2) monotonic convergence (MC), where the swimmers approach each other and reach a minimum distance at which near field interactions become more dominant over the far-field interactions, (3) convergence (C), where the swimmers attract each other after some transient behavior, (4) monotonic divergence (MD), where the distance between the swimmers increases monotonically as they move together, and (5) divergence (D), where the swimmers diverge after a transient attractive behavior. Figures 4(c)–4(f) depict the detailed state diagrams, the examples of the observed states are showed in Figs. 4(h)–4(l), and the corresponding distance as a function of time is plotted in Fig. 4(g).

The peculiar bounded state is a result of the system's chiral nature, which can be observed only for the asymmetric combination of two swimmers, i.e., either puller-pusher or pusher-puller. Except for the bounded state, the other states have also been reported for the simple swimmers that move either in a straight line or a circular path [39,61–63]. These states can be observed for either the symmetric or asymmetric combinations of two swimmers. Note that when the swimmers exhibit the monotonic convergence or convergence behavior, the distance reduces as they approach each other. Below a certain distance, the far-field approximation becomes inaccurate, and the near-field becomes dominant. A rigorous analysis of the near-field interaction between two chiral squirmers will be subjected to future work.

To investigate the robustness of the observed bounded states, we have considered various initial configurations of the swimmers. However, we have found that bounded states are observed only if the swimmers oriented approximately in parallel (side-by-side) configuration initially. For other initial conditions, the swimmers do not stay in proximity long enough to influence each other's motion. Therefore, the contact time between the swimmers is shorter, and they do not exhibit the bounded state. As the chiral squirmers move in helical trajectories, their  $x$  and  $y$  (planar) components of the helical trajectories oscillate as  $x(t) \simeq r_0 \sin(\Omega t)$  and  $y(t) \simeq r_0[1 - \cos(\Omega t)]$ , where  $r_0$  is the radius of the helix which is a function of velocity and rotation rate ( $\Omega$ ) of the chiral squirmer. During the bounded state, swimmers exhibit in-phase oscillations when they are close to each other and anti-phase oscillations when far away; see Fig. 5. Similar behavior can be observed for the  $y$  components of the flow field (not shown). Note that the observed bounded states are stable even with small perturbations to  $\lambda$  and  $\chi$  which are  $\epsilon_1 \sim 5v/24$  and  $\epsilon_2 \sim 0.01\pi/24$ , respectively.

The influence of initial distance between the swimmers on the bounded state is discussed in Sec. V. We have observed that the chiral paths but not the chiral flows influence the bounded state. Also, by setting  $\lambda_{1,2} = 0$ , i.e., in the absence of the  $l = 2$  modes in the flow field, swimmers become neutral (neither pullers nor pushers), and they move in their respective directions without changing their

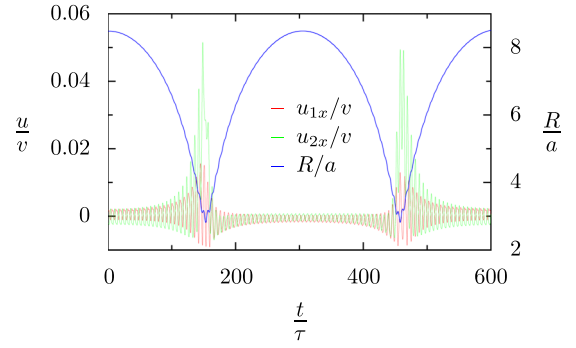


FIG. 5. Numerically obtained, the scaled  $x$  component of the flow field  $u_x$ , Eq. (6), and the scaled distance  $R$  between the swimmers as a function of scaled time  $t$  when the swimmers exhibit the bounded state.  $u_{1x}$  ( $u_{2x}$ ) corresponds to flow field of swimmer 1 (2) at the position of swimmer 2 (1). The parameter values are same as in Fig. 4(h).

orientations. A similar behavior is reported also for axisymmetric squirmers [62].

### B. State diagram in the $\lambda$ - $\lambda$ plane

In this case, we consider  $\chi_1 = \chi_2 = \pi/3$  and study the effect of the hydrodynamic field of one swimmer on the other. Figure 6 depicts the hydrodynamic behavior of two swimmers with varying  $\lambda_1$  and  $\lambda_2$ . We found that interaction depends on the swimmer type, i.e., pusher or puller set by the sign of  $\lambda_{1,2}$ . For example, for the choice  $\lambda = -\lambda_1 = \lambda_2$  swimmers exhibit a bounded state for the puller-pusher combination (see top right panel in Fig. 6) but show a monotonic divergence state for the combination of pusher-puller (see top left panel in Fig. 6). This altered behavior is because of the asymmetry in the flow patterns about the direction of motion exhibited by chiral swimmers of puller and pusher nature. Note that the flow pattern of an axisymmetric puller is mirror

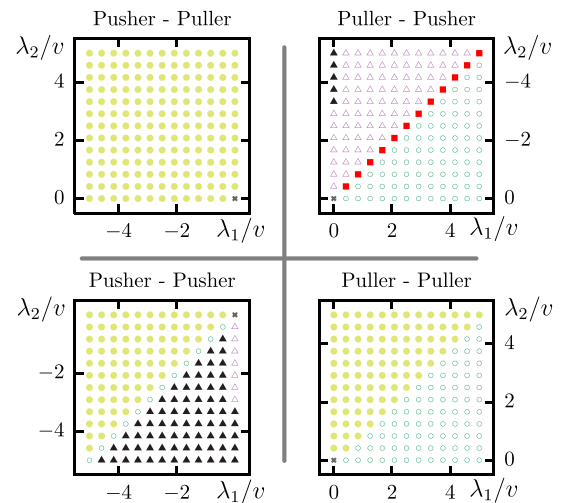


FIG. 6. Numerically obtained swimming behaviors of a pair of hydrodynamically interacting chiral squirmers, one with the strength  $\lambda_1$  and the other one with  $\lambda_2$ . Here we set  $\chi_1 = \chi_2 = \pi/3$ . Symbols are same as in Fig. 4.

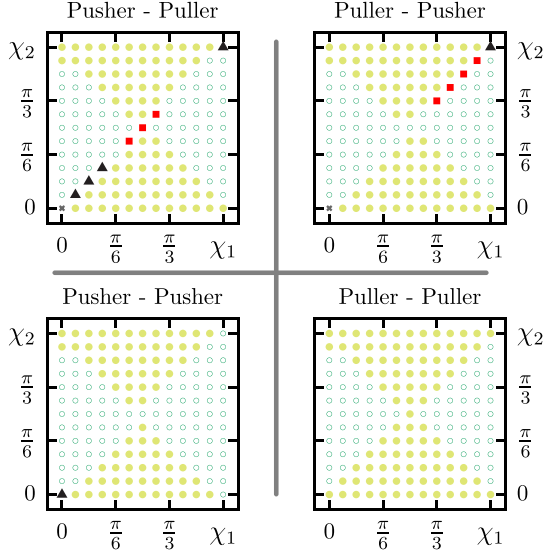


FIG. 7. Numerically obtained swimming behaviors of a pair of hydrodynamically interacting chiral squirmers, one with the orientation  $\chi_1$  and the other with  $\chi_2$ . Here we set  $|\lambda_1| = |\lambda_2| = v$ . Symbols are same as in Fig. 4.

symmetric, about the swimming direction, to the flow pattern of its counterpart, a pusher. However, in chiral swimmers, the flow patterns of puller and pusher are not mirror symmetric to each other. Thus, the puller-pusher combination gives a different behavior compared to the puller-pusher combination at fixed  $\lambda_1$  and  $\lambda_2$  values. The same is reflected in Fig. 6. Note that only puller-pusher combinations of chiral swimmers exhibit bounded states but not nonchiral swimmers. For the other combinations, i.e., pusher-pusher or puller-puller, depending on the strength of  $\lambda_1$  and  $\lambda_2$ , a pair of chiral swimmers exhibit the states such as C, MC, D, and MD. Similar states have been reported in the case of a pair of axisymmetric swimmers [39,61,62]. Also, note that the observed bounded states are stable even with a small perturbation  $\epsilon_1 \sim 5/24$  to  $\lambda_1$  and  $\lambda_2$ .

### C. State diagram in the $\chi$ - $\chi$ plane

Here we study the interaction between two swimmers by varying their respective initial angles between velocity and rotational axis, i.e.,  $\chi_{1,2}$  at time  $t = 0$ , by setting  $\lambda_1 = \lambda_2 = v$ . Varying  $\chi$  induces different directions of the rotational axis with respect to the velocity of the swimmer. Note that  $\chi$  does not influence the magnitude of swimmers' rotation rate; however, it influences the velocity field and vorticity. Therefore, when two swimmers interact hydrodynamically, their collective behavior is dictated by their respective  $\chi$  values. This gives rise to different swimming states; see Fig. 7. In a puller-pusher or pusher-puller combination, if the net rotation rates of both the swimmers are equal, i.e.,  $\chi_1 = \chi_2$ , the swimmers get attracted to each other, giving rise to either bounded or monotonic convergence states. If the net rotation rates are different, the swimmers mainly repel each other, giving rise to divergence and monotonic divergence states. Note that the observed bounded states are stable even with a small

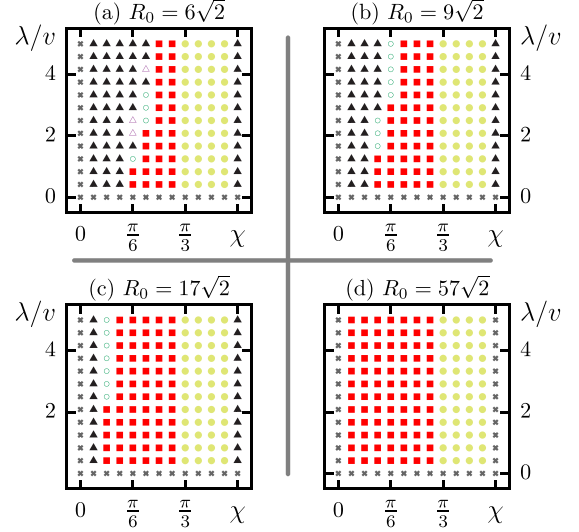


FIG. 8. Numerically obtained swimming behaviors of pusher-puller type chiral swimmers with different initial positions. The corresponding initial ( $t = 0$ ) distance is  $R_0$ . (a) For  $\mathbf{q}_1 = (9, 9, 0)a$  and  $\mathbf{q}_2 = (3, 3, 0)a$  [as in Fig. 4(e)], (b) for  $\mathbf{q}_1 = (12, 12, 0)a$  and  $\mathbf{q}_2 = (3, 3, 0)a$ , (c) for  $\mathbf{q}_1 = (20, 20, 0)a$  and  $\mathbf{q}_2 = (3, 3, 0)a$ , and (d) for  $\mathbf{q}_1 = (60, 60, 0)a$  and  $\mathbf{q}_2 = (3, 3, 0)a$ . Swimmers have the same initial velocity  $\mathbf{V}_1 = \mathbf{V}_2 = v(0, 0, 1)$  and rotation rate  $\mathbf{\Omega}_1 = \mathbf{\Omega}_2 = v(\cos \chi, 0, \sin \chi)/a$ , which depends on the angle  $\chi$ . Symbols are same as in Fig. 4.

perturbation  $\epsilon_2 \sim 0.01\pi/24$  to  $\chi_1$  and  $\chi_2$ . Interestingly, apart from the case  $\chi_1 = \chi_2$ , interaction of the squirmers flips about  $\chi_1 = \chi_2 = \pi/4$  and shows symmetric pattern; see Fig. 7.

## V. INFLUENCE OF THE INITIAL CONFIGURATION OF THE SWIMMERS

To get the stability of the observed states as a function of the initial ( $t = 0$ ) distance  $R_0$  between the swimmers, we consider a pair of pusher-puller type chiral swimmers as a test case. As before, we keep the initial velocity and rotation rate the same for both the swimmers and vary the initial distance between them (see Fig. 8). Interestingly, B and MD states are stable even with the varying distance between the chiral swimmers. For lower  $R_0$ , C and D states appear between the B and MC states [see Fig. 8(a)]. However, as  $R_0$  increases, swimmers exhibit mainly B and MD states. In general, the tendency of the swimmers is either repulsive or attractive. In purely repulsive situations, swimmers exhibit MD states. However, if swimmers tend to attract each other, the swimming behavior can be classified as C, MC, D, or B based on their far-field interactions. As  $R_0$  increases, the closest distance that the swimmers can approach increases. Accordingly, the nature of the interaction between swimmers changes with varying  $R_0$ . With increasing  $R_0$ , the flow field of the swimmers prohibits them from approaching close to each other. Thus, swimmers do not exhibit C and D states in this situation, leaving mainly B and MD states in the state diagram. For  $\chi = \pi/2$ , swimmers show attractive behavior at lower  $R_0$  values, and at higher  $R_0$ , they move parallel to each other. In the other combination of swimmers, e.g., pusher-pusher or

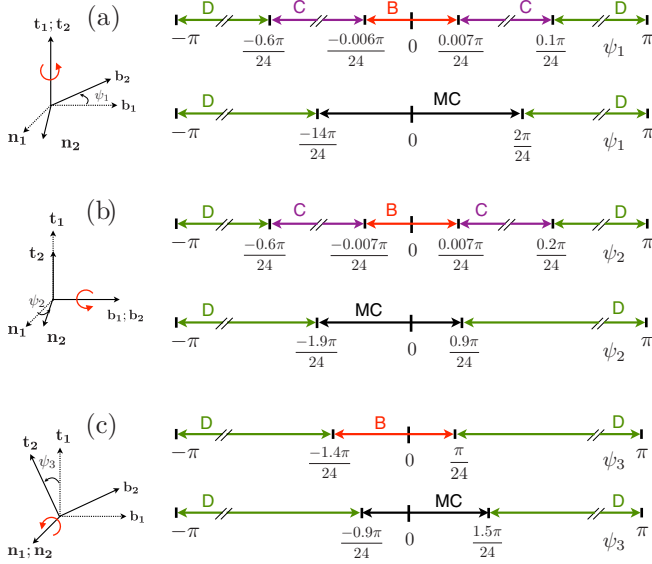


FIG. 9. [(a)–(c)] Stability of the bounded (B) and monotonic convergent (MC) states as a function of initial orientations at a fixed distance  $R_0 = 6\sqrt{2}$  between the swimmers. Note that the initial body frame of reference of swimmer 1 ( $\mathbf{n}_1, \mathbf{b}_1, \mathbf{t}_1$ ) is aligned with the laboratory-frame of reference. However, ( $\mathbf{n}_2, \mathbf{b}_2, \mathbf{t}_2$ ) of swimmer 2 is rotated with respect to the frame of swimmer 1. Rotation about  $\mathbf{t}_2$  axis is  $\psi_1$ , rotation about  $\mathbf{b}_2$  axis is  $\psi_2$ , and rotation about  $\mathbf{n}_2$  axis is  $\psi_3$ . For the B state we have chosen  $\lambda_1 = 2, \lambda_2 = -2$ , and  $\chi_1 = \chi_2 = \pi/3$ . For the MC state we have chosen  $\lambda_1 = -2, \lambda_2 = 2$ , and  $\chi_1 = \chi_2 = \pi/8$ .

puller-puller, MD states do not alter concerning  $R_0$ . However, for intermediate  $R_0$ , swimmers mostly remain in the D state. If  $R_0$  is very high, the swimmers never approach each other at a distance to interact effectively (gray cross states in the state diagrams). Note that for  $R_0 \sim 10^3$ , the hydrodynamic interaction becomes ineffective.

While throughout the study, we considered parallel swimming configurations, a question may arise how does the initial relative orientation of the swimmers influence the swimming dynamics and, in particular, the stability of various swimming states that they exhibit. We perturb the initial configuration by keeping one of the swimmers' body frame of reference ( $\mathbf{n}_1, \mathbf{b}_1, \mathbf{t}_1$ ) aligning with the laboratory frame ( $\mathbf{x}, \mathbf{y}, \mathbf{z}$ ) while the body frame of the other is rotated slightly. Rotation about  $\mathbf{t}_2$  axis is  $\psi_1$ , rotation about  $\mathbf{b}_2$  axis is  $\psi_2$ , and rotation about  $\mathbf{n}_2$  axis is  $\psi_3$ . We have observed that the perturbation in the orientations does not influence the D, MD, and C states much. However, it influences the B and MC states; see Fig. 9. Note that B and MC states are stable even with a small change in the initial relative orientations of the swimmers. For example, the bounded state is stable within the limits,  $(-0.006\pi/24) \leq \psi_1 \leq (0.007\pi/24)$ ,  $(-0.007\pi/24) \leq \psi_2 \leq (0.007\pi/24)$ , and  $(-1.4\pi/24) \leq$

$\psi_3 \leq (\pi/24)$ . Similarly, for the monotonic convergence state,  $(14\pi/24) \leq \psi_1 \leq (2\pi/24)$ ,  $(-1.9\pi/24) \leq \psi_2 \leq (0.9\pi/24)$ , and  $(-0.9\pi/24) \leq \psi_3 \leq (1.5\pi/24)$ . However, if the orientation angles are high, B and MC states are converted to divergence states.

## VI. CONCLUSIONS

Using the chiral squirmer model, a generalization of the well-known squirmer model, we have investigated the dynamic behavior of two chiral squirmers coupled hydrodynamically. A chiral squirmer exhibits a chiral asymmetry of the surface slip velocity due to which it has both linear and rotational motion. The coupling of linear and rotational motion of the swimmer leads to a helical swimming path. We found that when a pair of chiral squirmers interact hydrodynamically, they can exhibit various types of motion. We first reestablished the well-studied behaviors in the case of a pair of simple axisymmetric squirmers [39,61,62]. However, we found situations in which two swimmers entered a bounded state and moved jointly on helical paths. This situation is related to swimmers' chiral nature, and we found it only for the asymmetric combination of pusher and puller type swimmers. These behaviors might be related to the planar oscillatory movements reported for three-sphere swimmers, which also stem from rotational contributions in the hydrodynamic interactions but lack chirality [64]. Bound states of rotating swimmers have been previously reported for a pair of *Volvox* algae that rotate and interact hydrodynamically near a substrate in the presence of gravity [13–15]. In this case, the observed bounded states are due to the combined effect of hydrodynamic interaction between the spinning bodies, lubrication force between them when they close by, and the gravity. However, in the current study, the observed bounded states are because of the chiral nature of the swimmers and their corresponding helical trajectories. The significance of bounded motion lies in its possible role in fertilization in an adverse environment. Notably, throughout this work, we assume constant surface squirming motion or slip velocity. However, in general, microorganisms may alter their squirming velocity in the presence of a nearby microswimmer.

Our model could be applicable to study the migration and the collective behavior of ciliated microorganisms and artificial swimmers [33,65–68]. It can also be further extended to study chemotaxis [23,24,69] or phototaxis [44,70], where the hydrodynamically coupled active swimmers move against a chemical gradient or a light source. As in the case of sperm cells [23,24], the presence of an external stimulus may regulate the amplitudes of the slip velocity in the chiral squirmer model and may ultimately lead to steering towards a stimulus.

## ACKNOWLEDGMENTS

This work was supported by the Max Planck Society and the Indian Institute of Technology Kharagpur, India.

[1] M. J. Lighthill, *Commun. Pure Appl. Math.* **5**, 109 (1952).

[2] J. R. Blake, *J. Fluid. Mech.* **46**, 199 (1971).

[3] C. Brennen and H. Winet, *Annu. Rev. Fluid Mech.* **9**, 339 (1977).

- [4] G. T. Yates, *Am. Sci.* **74**, 358 (1986).
- [5] H. C. Berg, *Phys. Today* **53**(1), 24 (2000).
- [6] E. Lauga and T. R. Powers, *Rep. Prog. Phys.* **72**, 096601 (2009).
- [7] E. Lauga, *The Fluid Dynamics of Cell Motility* (Cambridge University Press, Cambridge 2020).
- [8] B. Alloul-Pinel and A. Ghadouani, in *The Spatial Distribution of Microbes in the Environment*, edited by R. B. Franklin and A. L. Mills (Springer, Dordrecht, 2007), p. 203.
- [9] M. E. Holwill, *Physiol. Rev.* **46**, 696 (1966).
- [10] T. L. Jahn and J. J. Votta, *Annu. Rev. Fluid Mech.* **4**, 93 (1972).
- [11] V. Magar and T. J. Pedley, *J. Fluid Mech.* **539**, 93 (2005).
- [12] S. Michelin and E. Lauga, *J. Fluid Mech.* **715**, 1 (2013).
- [13] K. Drescher, K. C. Leptos, I. Tuval, T. Ishikawa, T. J. Pedley, and R. E. Goldstein, *Phys. Rev. Lett.* **102**, 168101 (2009).
- [14] T. J. Pedley, D. R. Brumley, and R. E. Goldstein, *J. Fluid. Mech* **798**, 165 (2016).
- [15] T. Ishikawa, T. J. Pedley, K. Drescher, and R. E. Goldstein, *J. Fluid. Mech* **903**, A11 (2020).
- [16] L. A. Pratt and R. Kolter, *Mol. Microbiol.* **30**, 285 (1998).
- [17] A. Houry, R. Briandet, S. Aymerich, and M. Gohar, *Microbiology* **156**, 1009 (2010).
- [18] A. P. Berke, L. Turner, H. C. Berg, and E. Lauga, *Phys. Rev. Lett.* **101**, 038102 (2008).
- [19] G. J. Li and A. M. Ardekani, *Phys. Rev. E* **90**, 013010 (2014).
- [20] H. C. Berg, *Random Walks in Biology* (Princeton University Press, Princeton, 1993).
- [21] J. R. Howse, R. A. L. Jones, A. J. Ryan, T. Gough, R. Vafabakhsh, and R. Golestanian, *Phys. Rev. Lett.* **99**, 048102 (2007).
- [22] P. Romanczuk, M. Bär, W. Ebeling, B. Lindner, and L. Schimansky-Geier, *Eur. Phys. J. Special Topics* **202**, 1 (2012).
- [23] B. M. Friedrich and F. Jülicher, *Proc. Natl. Acad. Sci. U. S. A.* **104**, 13256 (2007).
- [24] B. M. Friedrich and F. Jülicher, *Phys. Rev. Lett.* **103**, 068102 (2009).
- [25] B. J. Nelson, I. K. Kaliakatsos, and J. J. Abbott, *Annu. Rev. Biomed. Eng.* **12**, 55 (2010).
- [26] D. Bray, *Cell Movements* (Garland, New York, 2001).
- [27] G. I. Taylor, *Proc. Roy. Soc. A* **209**, 447 (1951).
- [28] E. M. Purcell, *Am. J. Phys.* **45**, 3 (1977).
- [29] A. Shapere and F. Wilczek, *Phys. Rev. Lett.* **58**, 2051 (1987).
- [30] H. Machemer, *J. Exp. Biol.* **57**, 239 (1972).
- [31] M. Leonetti, *Europhys. Lett.* **32**, 561 (1995).
- [32] P. Lammert, J. Prost, and R. Bruinsma, *J. Theor. Biol.* **178**, 387 (1996).
- [33] R. Golestanian, T. B. Liverpool, and A. Ajdari, *Phys. Rev. Lett.* **94**, 220801 (2005).
- [34] N. Osterman and A. Vilfan, *Proc. Natl. Acad. Sci. USA* **108**, 15727 (2011).
- [35] J. Liu and H. Ruan, *Bioinspir. Biomim.* **15**, 036002 (2020).
- [36] M. Saadat, M. Mirzakanloo, J. Shen, M. Tomizuka, and M. Alam, in *Proc. American Control Conference, Philadelphia, PA, USA* (2019), p. 4478.
- [37] M. Schmitt and H. Stark, *Phy. Fluids* **28**, 012106 (2016).
- [38] M. Lisicki, S. Y. Reigh, and E. Lauga, *Soft Matter* **14**, 3304 (2018).
- [39] T. Ishikawa, M. P. Simmonds, and T. J. Pedley, *J. Fluid. Mech.* **568**, 119 (2006).
- [40] K. T. Wu, Y. T. Hsiao, and W. Y. Woon, *Phys. Rev. E* **98**, 052407 (2018).
- [41] J. Gray, *J. Exp. Biol.* **32**, 775 (1995).
- [42] C. J. Brokaw, *J. Exp. Biol.* **35**, 197 (1958).
- [43] H. C. Crenshaw, *Am. Zool.* **36**, 608 (1996).
- [44] G. Jékely, J. Colombelli, H. Hausen, K. Guy, E. Stelzer, F. Nédélec, and D. Arendt, *Nature Lett.* **456**, 395 (2008).
- [45] T. Yamamoto and M. Sano, *Phys. Rev. E* **99**, 022704 (2019).
- [46] T. Yamamoto and M. Sano, *Soft Matter* **13**, 3328 (2017).
- [47] T. Yamamoto and M. Sano, *Phys. Rev. E* **97**, 012607 (2018).
- [48] F. Fadda, J. J. Molina, and R. Yamamoto, *Phys. Rev. E* **101**, 052608 (2020).
- [49] E. Tjhung, M. E. Cates, and D. Marenduzzo, *Proc. Natl. Acad. Sci. USA* **114**, 4631 (2017).
- [50] L. N. Carenza, G. Gonnella, D. Marenduzzo, and G. Negro, *Proc. Natl. Acad. Sci. USA* **116**, 22065 (2019).
- [51] F. Lancia, T. Yamamoto, A. Ryabchun, T. Yamaguchi, M. Sano, and N. Katsonis, *Nat. Commun.* **10**, 5238 (2019).
- [52] O. S. Pak and E. Lauga, *J. Eng. Math.* **88**, 1 (2014).
- [53] G. M. Hallegraef, *Phycologia* **32**, 79 (1993).
- [54] T. J. Pedley and J. O. Kessler, *Annu. Rev. Fluid Mech.* **24**, 313 (1992).
- [55] T. J. Pedley and J. O. Kessler, *J. Fluid Mech.* **212**, 155 (1990).
- [56] I. Llopis and I. Pagonabarraga, *Eur. J. Phys. E* **26**, 103 (2008).
- [57] P. Friedl and D. Gilmour, *Nat. Rev. Mol. Cell Biol.* **10**, 445 (2009).
- [58] J. J. Tyson and J. D. Murray, *Development* **106**, 421 (1989).
- [59] J. Happel and H. Brenner, *Low Reynolds Number Hydrodynamics* (Springer, The Netherlands, 1983).
- [60] H. A. Stone and A. D. T. Samuel, *Phys. Rev. Lett.* **77**, 4102 (1996).
- [61] S. Michelin and E. Lauga, *Bull. Math. Biol.* **72**, 973 (2010).
- [62] I. Llopis and I. Pagonabarraga, *J. Non-Newtonian. Fluid. Mech* **165**, 946 (2010).
- [63] N. Yoshinaga and T. B. Liverpool, *Eur. Phys. J. E* **41**, 76 (2018).
- [64] C. M. Pooley, G. P. Alexander, and J. M. Yeomans, *Phys. Rev. Lett.* **99**, 228103 (2007).
- [65] R. F. Ismagilov, A. Schwartz, N. Bowden, and G. M. Whitesides, *Angew. Chem. Int. Ed.* **41**, 652 (2002).
- [66] R. Dreyfus, J. Baudry, M. L. Roper, M. Fermigier, H. A. Stone, and J. Bibette, *Nature (London)* **437**, 862 (2005).
- [67] W. Paxton, S. Sundararajan, T. E. Mallouk, and A. Sen, *Angew. Chem. Int. Ed.* **45**, 5420 (2006).
- [68] T. Hogg, *Auton. Agents Multi-Agent Syst.* **14**, 271 (2007).
- [69] R. Maity and P. S. Burada, *Eur. Phys. J. E* **42**, 20 (2019).
- [70] K. Drescher, R. Goldstein, and I. Tuval, *Proc. Natl. Acad. Sci. USA* **107**, 11171 (2010).